# Non-Newtonian flow effects during spin coating large-area optical coatings with colloidal suspensions

Jerald A. Britten and Ian M. Thomas
*Lawrence Livermore National Laboratory, Livermore, California 94550*

(Received 6 May 1991; accepted for publication 11 October 1991)

Multilayer sol-gel optical high reflectors with greater than 99% reflection have been prepared on substrates up to 20 cm in diameter by spin coating silica/alumina colloidal suspensions. These coatings are radially nonuniform, owing to the extensive shear-thinning rheology of the high-index alumina suspension. To a large degree the film thickness nonuniformity can be compensated for by the reflection bandwidth. The rheological properties of the alumina suspension under steady shear have been measured. The low-shear reduced viscosity and the shear-thinning time constant are shown to vary exponentially with $\phi^2$, where $\phi$ is the solids volume fraction. At $\phi = 0.1$ the sol has effectively gelled. A model for spincoating with a non-Newtonian fluid has been developed that uses the Carreau rheology model to fit the measured viscometric data. Modeling and experimental results show that as long as these non-Newtonian effects are sufficiently large (as in this case) the radial film uniformity is determined only by these parameters and cannot be significantly influenced by spin rate, initial solids fraction, or any other parameters under the control of the operator. However, most of the film thickness variation occurs in the first 1–2 cm from the substrate center, leaving the remainder almost uniform. Therefore the degree of nonuniformity does not appreciably increase with increasing substrate size.

## I. INTRODUCTION

Manufacture of large, laser-damage-resistant, dielectric, multilayer high reflectors (HRs) for high-power laser applications has traditionally been the province of electron-beam evaporation technology. Recently, however, sol-gel processing techniques have demonstrated the potential for making such mirrors at a significantly lower cost. Damage-resistant single-layer antireflective coatings on large optics have been made by sol-gel dip coating for several years.[1] In recent work Thomas[2] has demonstrated sol-gel quarter-wave interference mirrors made by spin coating multilayers on 5.1-cm-diam substrates. These mirrors reflect 1.06-$\mu$m light and meet laser damage threshold (40 J/cm$^2$ at 10 ns) and reflection ($>99\%$) specifications required by our application in laser-driven inertial confinement fusion experiments.

The work by Thomas[2,3] focused on identifying a suitable high-refractive-index material for the multilayer. The low-index layer is composed of $SiO_2$ spheres roughly 30 nm in diameter, which, when deposited, give an index of 1.22. This layer is deposited from a colloidal suspension in ethanol, similar to the suspensions from which antireflective coatings on silica substrates are made.[1] The criteria for choosing the high-refractive-index material were high-laser-damage threshold and ease of preparation of the sol. After investigating several possibilities, a sol consisting of plate-shaped hydrated alumina particles, roughly 300 nm across and 50 nm thick, in a methanol/water solvent was chosen. This material is made by reacting aluminum metal with sec-butanol, subsequently hydrolyzing the butoxide, redispersing the alumina with acid, and finally replacing some of the solvent water with methanol. Layers deposited from this suspension have a refractive index of 1.42–1.44. Typically, 18 layer pairs of $SiO_2$/AlOOH in a quarter-wave stack are sufficient to provide 99% reflection of the incident beam. Figure 1 shows a representative transmission spectrum for a $(AlOOH/SiO_2)^{18}$ HR made by spincoating.

The next issue to be addressed is scaleup of the process to larger optics, with maximum dimensions of up to 60 cm. This article reports on a combined experimental, characterization, and modeling study of scaleup issues arising from application of the spin-coating process to larger substrates. The focus of this work is on understanding the impact of rheological properties of the coating solutions on spin-coated film profiles. The rheological properties of the sols are measured and these measurements are used in a spincoating model in an effort to reproduce experimental results and predict the film thickness uniformity as a function of substrate radius.

## II. EXPERIMENT

Coatings were applied on silica substrates up to 20 cm in diameter, using an automated double-dispense spinner (Advanced Control Engineering, Santa Clara, CA.) Silica and alumina colloidal suspensions were prepared as described by Thomas.[1–3]

Uniform films across the entire substrate were possible with the silica sol. Application of a 3% (by weight) $SiO_2$ sol in ethanol at 50 rpm, followed by acceleration at nominally 6000 rpm/s to 1800 rpm produced a film of the desired quarter-wave thickness of 217 nm.

Films deposited from the alumina sol, however, consistently exhibited a decrease in thickness from center to edge, which persisted when water/methanol solvent ratios were changed, when methanol was replaced by methoxyethanol, and when airflow patterns were altered by

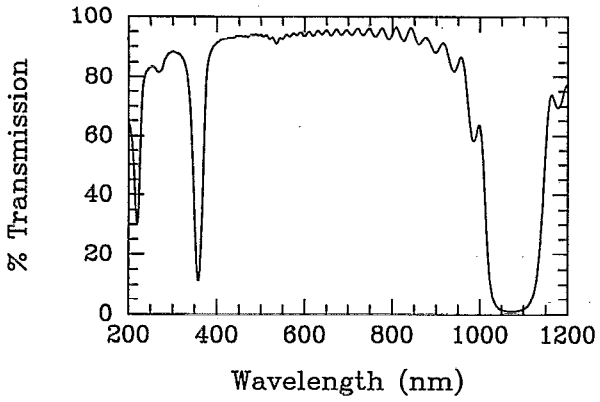


FIG. 1. Transmission spectrum of a ($SiO_2$/AlOOH) (Ref. 18) HR on a 20-cm substrate made by spin coating.

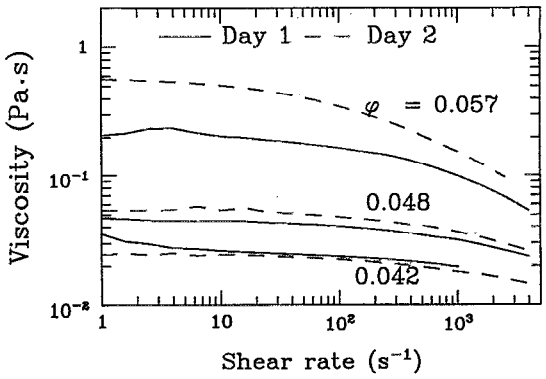


FIG. 3. Effect of aging of the alumina/water suspension on apparent viscosity.

shrouding. This radial variation was not noticed when spincoating on 5-cm substrates in earlier work.[2,3]

This nonuniformity was traced to non-Newtonian rheological properties of the alumina suspension. It is well known that nonuniform films can be expected from spinning non-Newtonian fluids.[4,5] Simple modeling suggested that spinning at lower rates decreases shear rates and results in a more uniform coating. Three HRs were made in which spin rates of 640, 1400, and 2400 rpm were used after application of the alumina sol, while applying the silica sol at the same rate. Radial film thickness profiles were measured spectrophotometrically by noting the wavelength of maximum reflection as a function of position. These profiles, normalized to account for slight calibration errors, are shown in Fig. 2. The spectrophotometer was not big enough to measure transmission close to the center of the 20-cm-diam substrate. Figure 2 shows that the effect of spin rate on the nonuniformity is insignificant over the substrate area measured. This is unfortunate, since the spin rate is the one variable that could be expected to influence this behavior. Other variables, such as relative humidity or initial solids volume fraction, affect film thickness uniformly over the entire substrate. Given this unexpected result, it was decided to characterize more completely the

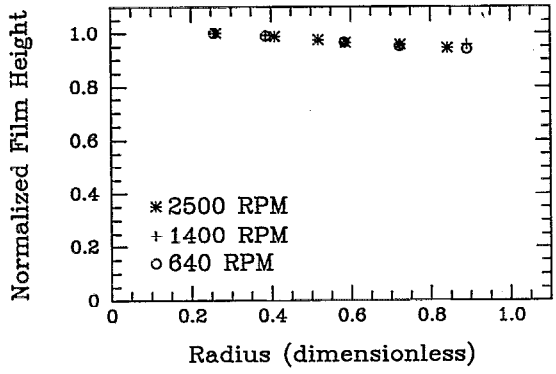


FIG. 2. Wavelength of maximum reflection vs radius on 20-cm-diam spin-coated HRs prepared at three different spin rates following alumina sol application. Normalized to have unit value at $r = 0.25$.

rheology of the alumina suspensions and use this information in a spincoating model to attempt to explain the observed behavior.

## III. RHEOLOGY CHARACTERIZATION

### A. Experiments

A Rheometrics Series 4 automated cone-and-plate viscometer was used to measure the apparent viscosity as a function of shear rate in alumina suspensions. The high-shear-rate limits of the measurements were defined by the maximum rotation speed of the plate (955 rpm) for the low-viscosity suspensions and by the maximum measurable torque for the case of high-viscosity suspension.

In practice the alumina sol is applied using an 80/20 ratio of methanol/water as the suspending fluid. This reduces surface tension for spreadability and the high volatility of the methanol allows us to use a dilute suspension that remains stable for long times. During spinning at high speed, the carrying fluid concentration varies from mostly methanol to mostly water. It was beyond the scope of our effort to characterize the entire water/methanol/alumina concentration space, and so we focus most of our attention on the alumina/water system, with some measurements of alumina/water/methanol suspensions as well as silica/ethanol suspensions included for comparison.

At the low solids loadings used for spin coating, the alumina sol remains fluid for a long period of time. However, it is thixotropic (it begins to gel) at higher concentrations such as those used in the rheological measurements. Figure 3 compares measurements taken within 6 h after preparation of the sol with measurements from the same sample aged approximately 20 h. This thixotropy is apparently not completely reversible, although the suspension does thin somewhat when subjected to steady high shear for several minutes. The measurements used in the modeling efforts described below were taken the same day the sol was prepared, but are undoubtedly influenced to some extent by gelation.

The sols at lower concentrations also sometimes exhibit a reversible anomalously high apparent viscosity at very low shear rates. This behavior is shown in Fig. 4. The

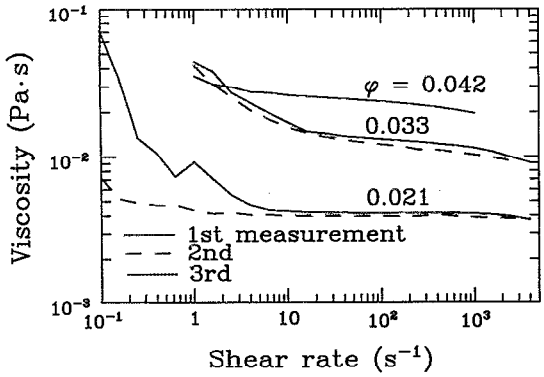


FIG. 4. Example of thixotropic behavior of alumina/water suspensions.

high viscosities at low shear rate are not consistently reproducible but in general disappear when the sample is spun for several minutes at high shear. The measurements are, however, quite reproducible at high shear rates for measurements taken not too far apart in time. Similar behavior has been reported for aqueous polystyrene suspensions containing dissolved polymer measured by Patel and Russel,[6] and is indicative of the shear-induced breakdown of a long-range structure in the sol. During spin coating, the suspension goes from very dilute to very concentrated in a few seconds, and thus it is assumed that there is no time for large-scale structure or order to develop. For these reasons, the subsequent rheology data are those taken from fresh samples subjected to high shearing flows for 2 or more minutes, and the anomalous high viscosity numbers at very low shears are discarded.

Figure 5 shows apparent viscosity versus shear-rate data for several samples of an alumina/water sol at different solids fraction. Also shown are solid lines representing a fit to the data that will be discussed later. The samples were prepared by weighing and converted to volume percent by assuming the density of the alumina was 3.15 (Boehmite) and neglecting any volume change due to solvation. It is apparent that both the apparent viscosity at low shear and the shear-thinning behavior are extremely sensitive to the solids fraction. In fact, at greater than 10% solids by

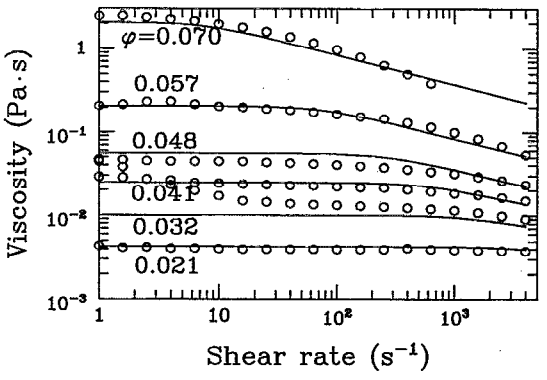


FIG. 5. Apparent viscosity of alumina/water suspensions as function of the solids volume fraction and the shear rate. Fit to the data is given by Eqs. (1) and (2).

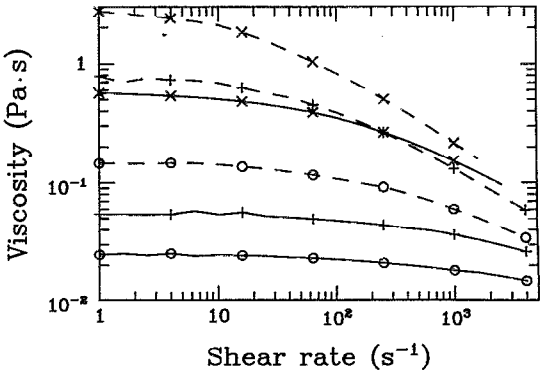


FIG. 6. Apparent viscosity of alumina/methanol/water suspensions compared with alumina/water systems with the same wt % alumina.—water; – –methanol; ○ 12.0 wt % alumina; + 13.7 wt %; × 16.0 wt %. Methanol/water ratio for the 12, 13.7, and 16-wt % alumina samples are 5/1, 5/2, and 5/3, respectively. These data taken after aging of the sols for about 24 h.

volume (26% by weight) the sol has effectively gelled. The sol can be stabilized to remain fluid at solid volume fractions approaching 10% by addition of acid, which acts to increase the charge on the particles and therefore increases repulsive forces. In principle, therefore, *p*H can be adjusted to reduce non-Newtonian rheology. Such a fix is not feasible in practice, however, since high-acid suspensions tend to resuspend and lift off previously deposited layers in our multilayer application.

The viscosity of the alumina sol in water/methanol solutions shows a higher degree of non-Newtonian behavior than with pure water. The apparent viscosity is equivalent at low solids concentrations, but increases with increasing methanol content at higher solids loadings. It is difficult to obtain rheology measurements at high solids loadings for the alumina/water/methanol system that are not highly influenced by the time-dependent gelation. Figure 6 compares apparent viscosity of alumina/water suspensions with alumina/methanol/water suspension with the same wt % alumina, but varying methanol/water ratios. The addition of a small amount of methanol produces a large increase in apparent viscosity. At the highest solids loading shown in Fig. 6, addition of 1 part methanol to 5 parts water increases the low-shear-rate viscosity by a factor of 5. This effect may be due to an increase in interparticle hydration forces which are less effectively screened by methanol than by water. Alternatively, it may be due to an effective increase in particle size as the particles become surrounded by methoxy groups rather than hydroxy groups as the methanol content increases.

The rheological behavior of the alumina suspensions contrasts markedly with that of the silica/ethanol suspension the same range in $\phi$. Figure 7 shows that the silica suspension exhibits substantially Newtonian behavior for $\phi$ up to at least 0.08. Einstein's[7] theory for the apparent viscosity of dilute noninteracting hard-sphere suspensions shows that $\eta = \mu/\mu_s = 1 + \frac{5}{2}\phi$. Experimental data for the viscosity of silica spheres in cyclohexane agree well with this limiting relation (see, e.g., de Kruif[8]). To agree with

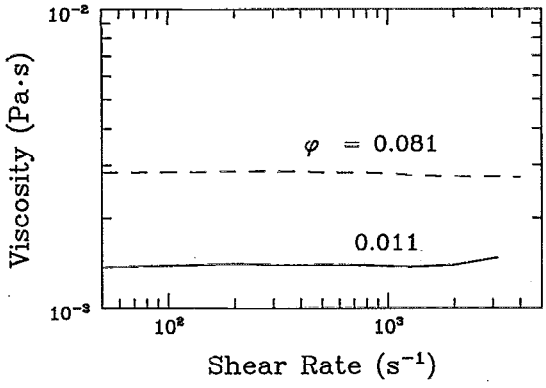


FIG. 7. Apparent viscosity of silica/ethanol suspensions as function of the solids volume fraction and the shear rate.

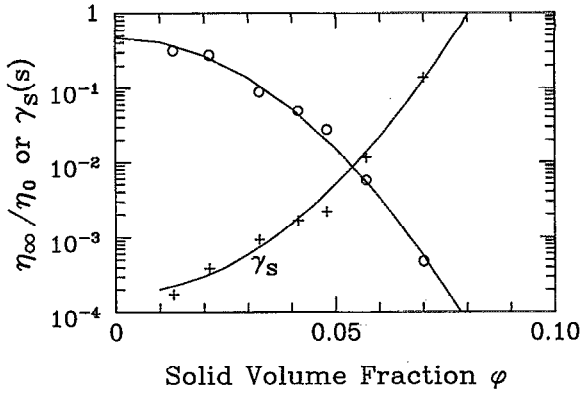


FIG. 8. Dependence of $\eta_0$ and $\gamma_s$ on $\phi$. Points are least-squares fit of raw data of Fig. 5 to Carreau equation, and solid lines represent the $\phi$ dependence given in Eq. (2).

the data of Fig. 7, the $\frac{5}{2}$ factor would need to be increased to 15. Recently Honig, Punt, and Offermans[9] reported deviations from the Einstein equation very similar to those seen here, for aqueous silica sols which were nonetheless Newtonian at low solids fractions with an apparent viscosity linear in $\phi$. They accounted for this behavior by including the size of the double layer surrounding the particles when they carry a charge. This so-called "primary electroviscous effect" is likely responsible for the rheological behavior of our silica sols as well. However, the forces involved are not sufficiently strong to cause shear thinning and thixotropy for $\phi < 0.1$.

### B. Model fitting

The Carreau constitutive equation (see Ref. 10), a very general relation characterizing the rheology of shear-dependent fluids, is used to fit the data of Fig. 5. When written in the form of an apparent viscosity, this relation takes the form

$$\eta=\frac{\mu}{\mu_s}=\eta_0\left(\frac{\eta_\infty}{\eta_0}+\frac{1-(\eta_\infty/\eta_0)}{(1+\gamma_s^2\dot{\gamma}^2)^{(n-1)/2}}\right)\dot{\gamma}, \tag{1}$$

where $\mu_s$ is the viscosity of the carrying fluid, $\eta_0$ and $\eta_\infty$ are the viscosities relative to $\mu_s$ at zero and infinite shear rate, respectively, $\gamma$ and $n$ quantify the shear-rate dependence, and $\dot{\gamma}$ is the shear rate. The exponent in the denominator $(n-1)/2$ is written such that this relation reduces to the familiar power-law viscosity model at high shear rates. For the spin-coating problem $\dot{\gamma}=\partial v_r/\partial z$ where $v_r$ is the radial fluid velocity and $z$ the axial dimension. Also, $\eta_0$, $\eta_\infty$, and $\gamma_s$ are, in general, functions of $\phi$ and are thus time dependent due to the drying of the film. To orient these parameters to the data shown in Fig. 5, $\eta_0$ characterizes the increase in apparent viscosity at low shear rates as $\phi$ increases, $\gamma_s$ and $n$ characterize the slope in viscosity versus shear-rate profile at intermediate shear rates, and $\eta_\infty$ characterizes the limiting viscosity ar very large shear rates.

To fit the data to this function we assume that $\eta_\infty$ can be taken as a constant independent of $\phi$ over the narrow $\phi$ range of interest. It is assigned the value 1.2, based on the low- and high-shear-viscosity values measured for $\phi = 0.0212$. The data of Fig. 5 was fitted to Eq. (1) to determine $\eta_0$, $n$, and $\gamma_s$. The functional dependence on $\phi$ was then determined from these values. The best fit was given by

$$\begin{aligned}&\eta_0=0.47\exp(1361\phi^2), \quad \eta_\infty=1.2,\\ &\gamma_s^2=3\times10^{-8}\exp(2765\phi^2), \quad n=0.644.\end{aligned} \tag{2}$$

Figure 8 shows the data and the calculated fit of $\eta_0$ and $\gamma_s$. The extreme dependence on $\phi$ of these parameters is striking. The suspension viscosity increases by almost 3 orders of magnitude as $\phi$ increases from 1% to 7%. Also, the shear-thinning parameter $\gamma_s^2$ increases by 6 orders of magnitude over this range. The fit breaks down for very small values of $\phi$, since $\eta_0$ should be unity for $\phi=0$ and linear in $\phi$, but the initial concentration of the suspensions applied during spin coating fall into the range represented by this fit. The $\phi^2$ dependence suggested by the data is significant, since this order represents interparticle interactions as dominating the rheological behavior. Exponential dependence of rheological properties on suspension volume fraction has been reported before for aqueous polystyrene suspensions with a nonadsorbing polymer added.[11] This has been attributed to formation of long-range ordered structure in the quiescent dispersion which break up in the presence of a shear field and subsequently interact with each other.

## IV. SPIN-COATING MODEL

An appropriate spin-coating model must include non-Newtonian film flow and evaporation to characterize the radial uniformity of the final film. We start with the model developed by Sukanek,[12] to which we have added non-Newtonian fluid flow effects described by the Carreau model discussed previously. This viscosity model in the context of rotating-disk flow was apparently first considered by Jenekhe and Schuldt.[5] Quite recently, Sukanek,[13] has extended his model to include non-Newtonian effects in a development identical to this one.

The lubrication approximation first employed by Emslie, Bonner, and Peck,[14] is the basis of the fluid flow

model. This approximation assumes that the gradient in shear stress in the axial direction is balanced by centrifugal acceleration in the film, with all other terms in the fluid momentum balance neglected. It is clearly not valid for early times in the transient flow when inertial effects are important.[15] However, the final film height is not affected by this early behavior, and the non-Newtonian flow effects do not come into play significantly until the high-shear lubrication approximation conditions are valid. Sukanek's model averages solvent concentration axially across the thickness of the film. This is felt a reasonable simplification for our application, and will be discussed further below in the context of evaporation.

Using scale factors from Sukanek's development,[12] dimensionless equations for the evolution of the film height $y$ and the axially averaged solvent volume fraction $\bar{x}$, obtained from the liquid and solid species balance equations, can be written as functions of the time $\tau$ and the radial coordinate $r$ as

$$\frac{\partial y}{\partial \tau} = -\frac{1}{r}\frac{\partial}{\partial r}(rq) - e(\bar{x}), \tag{3}$$

$$\frac{\partial \bar{x}}{\partial \tau} = -\frac{q}{y}\frac{\partial \bar{x}}{\partial r} - \frac{(1-\bar{x})}{y}e(\bar{x}). \tag{4}$$

In the above equations $e(\bar{x})$ is the dimensionless evaporation rate and the local volumetric flowrate $q$ is the integral of the radial velocity $v_r$ across the film:

$$q = \int_0^y v_r\, dz, \tag{5}$$

where $z$ is the axial direction.

An equation for the radial velocity can be written in terms of the Carreau model with assumption of zero shear at the liquid/gas interface as

$$\frac{dv_r}{dz} = \frac{r(z-y)}{\eta_0\{(\eta_\infty/\eta_0) + 1 - (\eta_\infty/\eta_0)/[1 + W^2(dv_r/dz)^2]^{(n-1)/2}\}}, \tag{6}$$

with the boundary condition $v_r(r=0) = 0$.

The reader is referred to Refs. 12 and 13 for further details on the derivation of these model equations.

For a Newtonian fluid Eq. (5) reduces to

$$q = ry^3/\eta(\phi). \tag{7}$$

The utility of this formulation is due to the small number of dimensionless parameters that arise. These are the dimensionless initial film height,

$$y_0 = h_0(k\nu_0)^{-1/3}\omega^{1/2}, \tag{8}$$

the initial solvent concentration $\bar{x}_0$, the shear-viscosity exponent $n$, and the shear-thinning parameter $W$ in Eq. (6),

$$W = \gamma_s R\omega^{3/2}k^{1/3}\nu^{-2/3}. \tag{9}$$

In the above, $\nu$ is the liquid kinematic viscosity, $h_0$ is the dimensional initial film height, $R$ the substrate radius, and $k$ is a mass-transfer coefficient defined below. $W$, properly identified as a Weissenberg number,[16,17] is the only parameter in the model equations containing the substrate radius. This dimensionless number is identical to that defined as a Deborah number in Sukanek's recent work[13] (the 2/3 exponent on $\omega$ in Ref. 13 is a typographical error). The time scale identified in the above equations is given by $\nu_0^{1/3}k^{-2/3}\omega^{-1}$.

Sukanek's formulation assumes the evaporation rate $e(\bar{x})$ to be proportional to the average solvent concentration across the film. However, in our system the presence of the depositing film offers no significant resistance to drying during the time the radial thickness profile is established. This can be understood by observing from the rheological data that the film ceases to flow significantly for solvent fractions of about 90%. Thus the drying can be taken to be analogous to that of a pure solvent film and we take the approach of Meyerhofer[18] and assume the drying rate to be a constant. Assuming a negligible solvent vapor pressure in the ambient air, the evaporation rate in dimensional terms $e^* = k\omega^{1/2}C_l$ is given by the well-known relation for mass/heat transfer at a spinning disk,[19,20] where $C_l$ is the solvent concentration in the liquid, $\omega$ the rotation rate in rad/s, and $k$ (units of cm/s$^{1/2}$) is given by

$$k = CDMP_s/\rho_l\nu_{air}^{1/2}RT. \tag{10}$$

In the above, $D$ is the binary diffusion coefficient of the solvent in air, $M$ the solvent molecular weight, $P_s$ the solvent vapor pressure, $\nu_{\text{air}}$ the air kinematic viscosity, $R$ the gas constant, $T$ the temperature, $\rho_l$ the liquid density, and $C$ a constant determined by solution of the flow equations[19,20] that is dependent on the solvent Schmidt number $\text{Sc} = \nu_{\text{air}}/D$. For our solvent vapors in air, $\text{Sc} \approx 1$ so $C = 0.4$. In dimensionless form in Eqs. (3) and (4), $e(\bar{x}) = 1$.

Equations (3) and (4) are discretized in the $r$ direction using centered differences over 21 equally spaced node points, and solved as a set of initial value ordinary differential equations in time, using the solver LSODE.[21] At each location and for each time step, the radial flowrate $q$ is evaluated by integrating Eq. (6) with a Runge–Kutta scheme using Newton iteration to evaluate the velocity gradient at each of 21 points along the $z$ direction from the substrate $z = 0$ to the film surface $z = y$. The resulting velocity profile $v_r(z)$ is integrated using Simpson's rule to obtain $q$. This solution scheme was checked against graphical results of a model of Jenekhe and Schuldt[5] which solves the fluid flow equations without evaporation and with constant values for the shear-thinning parameters.

TABLE I. Parameter values for spin-coating simulation.

| | |
|---|---|
| Kinematic viscosity $\nu_0$ (cm$^2$/s) | 0.01 |
| Evaporation constant $k$ (cm/s$^{1/2}$) | $6.2\times10^{-6}$ |
| Initial film height $h_0$ (cm) | 0.046 |
| Substrate radius $R$ (cm) | 7.6 |
| $y_0$ (dimensionless) | 95 |
| Initial solids weight fraction | 0.09 |

Predicted film height profiles agreed to within 2% for the longest times and largest shear-thinning parameter values shown in their paper.

The solution of Eqs. (3) and (4) is continued in time until at time $t_{end}$ everywhere on the substrate the ratio of the film thinning due to evaporation to that due to centrifugal flow is greater than $10^4$. The final film thickness depends on the unknown details of the solids packing, but we are only interested here in the relative radial uniformity. Therefore we need only assume that the final local thickness is proportional to the local film height multiplied by the local solids fraction at $t_{end}$. The general behavior of this system at a given time is such that the film height decreases from center to edge, while the solids volume fraction $(1-\bar{x})$ increases, but less strongly, such that their product $y(1-\bar{x})$ decreases slightly from center to edge.

## V. RESULTS AND DISCUSSION

To compare model predictions with experimental data, single layers were spun on 16-cm-diam substrates using a 9% (by weight) alumina/water suspension at different spin speeds. Rheological parameters measured as described above and other parameter values corresponding to water as the carrier solvent were used to simulate the experiments. These parameter values are given in Table I.

The normalized radial film thickness variation calculated for simulations corresponding to spin rates of 750, 1500, and 2500 rpm are compared with measured profiles on an expanded scale in Fig. 9. The predicted film thickness agrees fairly well with that measured near the edge of the disk, but the predicted profiles show more curvature at large radius, whereas in the measured profiles the nonuniformity is concentrated near the center of the disk, and the profile is relatively flat for large $R$. Possible reasons for this discrepancy are several, but as discussed below, it is felt that uncertainty in the rheological parameters is the most likely cause, and the experimental profiles can be reproduced if a more highly non-Newtonian rheology is assumed.

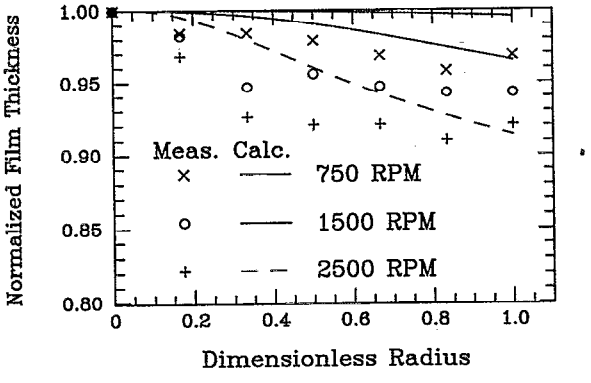


FIG. 9. Calculated and measured film thickness profiles, normalized at $r=0$, for single layers deposited from alumina/water sols at three different spin rates.

The lubrication flow assumption is considered to be quite appropriate in this case. The time in which inertial effects are important is extremely short due to the rapid thinning of the film. Also, during this time the dilute suspension is almost Newtonian and thus these effects would not influence the radial film uniformity. Uncertainty in initial conditions are similarly not believed to influence the final results, since, as found by Sukanek,[13] and others, the final film thickness at the time of gelation is essentially independent of $y_0$ as long as it is sufficiently large. Inclusion of a finite acceleration to the final speed (nominally 6 krpm/s) would, if anything, result in a more uniform calculated profile, since the film would be exposed to lower shear rates initially. The validity of the uniform mass-transfer model for these conditions of laminar flow of the air above the spinning disk is well established. Results do not change when an evaporation rate linear in the solvent volume fraction, instead of a constant rate, is used, because the profile is established at such high solvent volume fractions.

The experimental profiles suggest that the sol is more non-Newtonian than rheological measurements indicate. There is a substantial uncertainty in the rheological parameters, which change drastically over a small volume fraction range, and in the initial volume fraction itself. Also, the sol used to deposit the layers shown in Fig. 9 had aged for 2–3 weeks, whereas the viscosity measurements were done with a fresh sol. The sols are nominally stable at low solids loadings, but some increase in apparent viscosity may have occurred. The shape of the calculated profiles changes as the shear-thinning parameter $W$ increases, in that the nonuniformity becomes concentrated near the center of the substrate while away from the center the profile remains relatively flat. An increase in the value of $n$, on the other hand, shifts the region of greatest thickness gradient farther out on the substrate and causes greater curvature at large radius, which is contrary to the observed profiles. Based on this observation, simulations were done for cases identical to those shown in Fig. 9 except that the value of $\gamma_s$ was increased by a factor of 3 and the initial solvent volume fraction was increased to 0.93. Calculated results of this simulation agree very closely with the experimental profiles of Fig. 9. Uncertainty in the $\phi$ dependence of the apparent viscosity thus appears to account for the discrepancy shown.

The variation in coating thickness that can be tolerated requires knowledge of how a systematic thickness variation in one of the coatings in a multilayer affects both the wavelength of maximum reflection $\lambda_{max}$ and the reflectance bandwidth $\Delta\lambda$ of the coating. Calculations using a commercially available optical thin film design software pack-

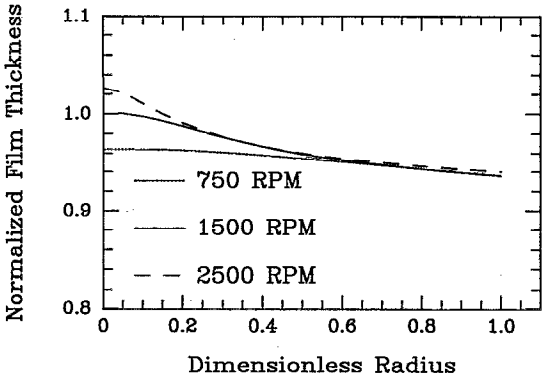


FIG. 10. Calculated variation in peak reflection wavelength ($\frac{1}{2}$ the physical thickness variation) for three simulated spinning speeds and conditions of Table I except that $\gamma_s$ is increased by 4×. These profiles are normalized to have the same value (that of the 1500-rpm case) at $r = 0.8$.

age (FILMCALC, FGT Software Association, Princeton, NJ) show that the percentage change in $\lambda_{max}$ corresponding to a systematic change $\Delta d$ in thickness of one of the layer pairs in a multilayer goes as

$$\Delta\lambda_{max}/\lambda_{max} = 0.5\Delta d/d_0, \tag{11}$$

where $d_0$ is the design thickness. The reflection bandwidth is governed by the index difference of the layers and the number of layers. The maximum reflectance bandwidth for a quarter-wave stack is given by[22]

$$\Delta\lambda = \lambda_{max}\frac{4}{\pi}\sin^{-1}(n_h - n_l)/(n_h + n_l), \tag{12}$$

where $n_h$ and $n_l$ are the high- and low-refractive indices, respectively. For our case $\Delta\lambda = 111$ nm. Calculations made with FILMCALC show that 25 layer pairs give a bandwidth that is 85% of the theoretical limit, and many additional layers are required to significantly increase the bandwidth past this value. Theoretically, therefore, 25 layer pairs giving a 99% reflection bandwidth of 94 nm can compensate for physical film thickness variations ±8% from the design thickness, which correspond to shifts in $\lambda_{max}$ of ±4%. The measured profiles shown in Fig. 2 fall in this range. In practice, however, 99% reflection bandwidths have been much narrower than theoretically predicted. The maximum $\Delta\lambda$ for $(AlOOH/SiO_2)^{25}$ HRs was found to be about 55 nm. This reduces the usable area on a 20-cm-diam substrate to about 75%. The reduction in bandwidth from theoretical could be the result of some interpenetration of the layers which acts to reduce the effective $\Delta n$ of the multilayer.

Recall from Fig. 6 that the non-Newtonian behavior of the sol increased substantially with methanol content. Since the HRs are made using an alumina/methanol/water system, we performed simulations in which $\gamma_s$ was increased by a factor of 4 to investigate the effects of spin rate on multilayers. Figure 10 shows the calculated profile for three spin speeds, adjusted to have a common value (that of the profile at 1500 rpm) at $r = 0.8$. This normalization point is chosen because spin speed and solids concentration were adjusted to give the desired reflection spectrum by spectrophotometric calibrations at this location during coating runs. Since the calculations compute a physical thickness, the center-to-edge variation has been halved in the profiles of Fig. 10 to mimic a corresponding shift in $\lambda_{max}$ as described by Eq. (11) above. These profiles are virtually indistinguishable for $r > 0.4$ and within 1.5% for $r > 0.3$. It is only near the substrate center that profiles at widely differing spin rates begin to diverge. This result identifies the reason why the optically measured profiles for the HRs shown in Fig. 2 did not depend on the spin speed over the substrate area examined. It shows that for a sufficiently extensive shear-thinning suspension, increasing the spin speed increases the overall thickness nonuniformity, but concentrates it near the center such that a large fraction of the substrate is unaffected.

The above analysis does not take into account turbulence effects generated by the rotating disk, which can act to increase the drying rate at outer regions of the substrate as the radius and/or spin rate are increased. The transition to turbulent flow adjacent to a rotating disk begins at a disk Reynolds number $\mathrm{Re} = r^2\omega/\nu$ of approximately $2\times10^5$, where $\nu$ is the kinematic viscosity of air at ambient conditions.[19,23] For a spin rate of 1500 rpm this corresponds to a substrate radius of approximately 14 cm. The evaporation rate for laminar flow in the air stream above the disk is independent of radius, as mentioned above. For turbulent flow, however, the average drying rate becomes proportional to $r^{0.8-0.9}$. This effect in principle can act to counteract the shear-thinning effect to produce a more uniform film on a large substrate. Therefore the analysis based on laminar flow is felt to be conservative.

## VI. CONCLUSIONS

The radial nonuniformity of silica/alumina quarter-wave reflective coatings arises from the non-Newtonian rheology of the alumina suspension. This rheology is influenced by interparticle attractive forces, which cause shear-thinning behavior which varies exponentially with the square of the solid volume fraction. The non-Newtonian behavior can be significantly reduced by lowering the *p*H of the sol, but this adjustment is not feasible in our multilayer application since the acid sol resuspends previously deposited layers and lifts off the coating.

A model for spin coating of a shear-thinning fluid has been developed using measured rheological data. Spectrophotometrically measured film thickness data as well as model calculations show that for highly shear-thinning sols the radial thickness variation is not influenced by the spin rate or other operator-controllable parameters except for a small region (1–2 cm) near the center of the substrate. Therefore, the nonuniformity can be compensated for over most of the substrate area by the reflection bandwidth, and the degree of nonuniformity does not increase significantly as the substrate radius increases.

## ACKNOWLEDGMENTS

This work was performed under the auspices of the U.S. Department of Energy by Lawrence Livermore National Laboratory under Contract No. W-7405-Eng-48.

[1] I. M. Thomas, Appl. Opt. **25**, 1481 (1986).
[2] I. M. Thomas, Appl. Opt. **28**, 4013 (1989).
[3] I. M. Thomas, Proc. SPIE **1438**, 484 (1990).
[4] A. Acrivos, M. J. Shah, and E. E. Petersen, J. Appl. Phys. **31**, 963 (1960).
[5] S. A. Jenekhe and S. B. Schuldt, Ind. Eng. Chem. Fundam. **23**, 432 (1984).
[6] P. D. Patel and W. B. Russel, J. Colloid Interface Sci. **131**, 201 (1989).
[7] A. Einstein, *Investigations on the Theory of Brownian Movement* (Dover, New York, 1956).
[8] C. G. de Kruif, E. M. F. van Irsel, A. Vrij, and W. B. Russel, J. Chem. Phys. **83**, 4717 (1986).
[9] E. P. Honig, F. J. Punt, and P. H. G. Offermans, J. Colloid Interface Sci. **134**, 169 (1990).
[10] R. I. Tanner, *Engineering Rheology* (Oxford University Press, Oxford, 1985), Chap. 1.
[11] P. D. Patel and W. B. Russel, J. Rheology **31**, 599 (1987).
[12] P. C. Sukanek, J. Imaging Tech. **11**, 184 (1985).
[13] P. C. Sukanek, J. Electrochem. Soc. **138**, 1712 (1991).
[14] A. G. Emslie, F. T. Bonner, and L. G. Peck, J. Appl. Phys. **29**, 858 (1958).
[15] T. J. Rehg and B. G. Higgins, Phys. Fluids **31**, 1360 (1988).
[16] C. J. Lawrence and W. Zhou, J. Non-Newtonian Fluid Mech. **39**, 137 (1991).
[17] M. J. Crochet, A. R. Davies, and K. Walters, *Numerical Simulation of Non-Newtonian Flow* (Elsevier, Amsterdam, 1984), pp. 41–42.
[18] D. Meyerhofer, J. Appl. Phys. **49**, 3993 (1978).
[19] F. Kreith, J. H. Taylor, and J. P. Chong, J. Heat Transfer **81**, 95 (1959).
[20] E. M. Sparrow and J. L. Gregg, J. Heat Transfer **81**, 249 (1959).
[21] A. C. Hindmarsh, ACM-Signum News **4**, 10 (1980).
[22] H. A. Macleod, *Thin Film Optical Filters* (Macmillan, New York, 1986), p. 170.
[23] N. Gregory, J. T. Stuart, and W. S. Walker, R. Soc. London Philos. Trans. **248**, 155 (1955).